Mineralogical Magazine, October 2010, Vol. 74(5), pp. 871–885

A temperature-dependent structure study of gem-quality hibonite from Myanmar

M. NAGASHIMA[1,2,*], T. ARMBRUSTER[1] AND T. HAINSCHWANG[3]

[1] Mineralogical Crystallography, Institute of Geological Sciences, University of Bern, Freiestrasse 3, CH-3012, Bern, Switzerland

[2] Department of Earth Science, Graduate school of Science and Engineering, Yamaguchi University, Yamaguchi 753-8512, Japan

[3] Laboratory for Gemstone Analysis and Reports, Gewerbestrasse 3, FL-9496 Balzers, Principality of Liechtenstein

[*Received 1 September 2010; Accepted 1 October 2010*]

ABSTRACT

The structure of hibonite from Myanmar (space group $P6_3/mmc$, $Z = 2$, at room temperature $a = 5.5909(1)$, $c = 21.9893(4)$ Å), with simplified formula $CaAl_{12}O_{19}$ and composition $(Ca_{0.99}Na_{0.01})_{\Sigma 1.00}(Al_{10.74}Ti_{0.52}\ Mg_{0.51}Zn_{0.11}Si_{0.08}Fe^{2+}_{0.04})_{\Sigma 12.00}O_{18.97}$, was investigated between temperatures of 100 K and 923 K by single-crystal X-ray diffraction methods. Structure refinements have been performed at 100, 296, 473 and 923 K. In hibonite from Myanmar, Ti substitutes for Al mainly at the octahedral Al4 site and, to a lesser degree, at the trigonal bipyramidal site, Al2. The Al4 octahedra build face-sharing dimers. If Ti^{4+} substitutes at Al4, adjacent cations repulse each other for electrostatic reasons, leading to off-centre cation displacement associated with significant bond-length distortion compared to synthetic (Ti-free) $CaAl_{12}O_{19}$. Most Mg and smaller proportions of Zn and Si are assigned to the tetrahedral Al3 site. 12-coordinated Ca in hibonite replaces oxygen in a closest-packed layer. However, Ca is actually too small for this site and engages in a 'rattling-type' motion with increasing temperature. For this reason, Ca does not significantly increase thermal expansion coefficients of hibonite. The expansion of natural Ti,Mg-rich hibonite between 296 and 923 K along the x and the z axes is $\alpha_a = 7.64 \times 10^{-6}\ K^{-1}$ and $\alpha_c = 11.19 \times 10^{-6}\ K^{-1}$, respectively, and is thus very similar to isotypic, synthetic $CaAl_{12}O_{19}$ and $LaMgAl_{11}O_{19}$ (LMA).

KEYWORDS: hibonite, hexa-aluminate, thermal expansion, crystal structure.

Introduction

HIBONITE, $CaAl_{12}O_{19}$, or calcium hexa-aluminate ($CaO{\cdot}6\ Al_2O_3 = CA_6$), is an oxide mineral of the magnetoplumbite group (space group $P6_3/mmc$, $Z = 2$) with considerable variation in its chemical composition (Curien *et al.*, 1956; Bermanec *et al.*, 1996).

In terrestrial environments, hibonite is rather rare and has, to our knowledge, only been reported from following localities: (1) Tranomaro, Madagascar (Curien *et al.*, 1956; Rakotondrazafy *et al.*, 1996); (2) Gornaya Shoriya, Siberia (Kuzmin, 1960; Yakovlevskaya, 1961); (3) the Furua Complex, Tanzania (Maaskant *et al.*, 1980); (4) near Punalur, South India (Santosh *et al.*, 1991; Sandiford and Santosh, 1991); (5) Mg-Al skarn, Handan-Xingtai area, China (Cao *et al.*, 1997); (6) the Chyulu Hills, Kenya Rift, Kenya (Ulianov *et al.*, 2005; Ulianov and Kalt, 2006); and (7) probably Mogok, Myanmar (Hainschwang *et al.*, 2010; this study). Hibonite from Myanmar is associated with corundum and minor unidentified Cu-Al-O and Cu-Al-Mg-Si-O phases. In general, hibonite

* E-mail: nagashim@yamaguchi-u.ac.jp
DOI: 10.1180/minmag.2010.074.5.871

forms under high-grade metamorphism, from upper amphibolite to granulite facies.

Apart from its rare terrestrial occurrences, hibonite is known in meteorites and interplanetary microspherules in chondrites (*e.g.* Keil and Fuchs, 1971; Burns and Burns, 1984; Bischoff *et al.*, 1985; Fahey *et al.*, 1987; Kimura *et al.*, 1993; Russell *et al.*, 1998; Nakamura *et al.*, 2007; Simon *et al.*, 2006). Several isotopic studies have been carried out on hibonite (*e.g.* Liu *et al.*, 2006; Simon *et al.*, 2006; Liu *et al.*, 2007; Stroud *et al.*, 2008; Liu *et al.*, 2009; Liu and McKeegan, 2009; Makide *et al.*, 2009) because it is thought to be one of the earliest solids in the solar system, occurring either as a condensate or as a refractory residue. The Fe^{2+}-dominant analogue, hibonite-(Fe), (Fe, Mg)$Al_{12}O_{19}$, was recently reported as a secondary alteration product of primary hibonite from the Allende meteorite (Ma, 2010).

All terrestrial samples, except for a few grains from Kenya analysed by Ulianov *et al.* (2005), show the substitution Ti^{4+} + (Mg^{2+},Fe^{2+}) → 2 Al^{3+}. TiO_2 concentrations may be as high as 10 wt.% (Santosh *et al.*, 1991). This substitution is also common in meteoritic hibonite. Terrestrial samples, except those from Siberia (Yakovlevskaya, 1961), the rims of the Punalur hibonite (Santosh *et al.*, 1991), and the hibonite from Kenya (Ulianov *et al.*, 2005), have the additional substitution mechanism REE^{3+} + (Mg^{2+}, Fe^{2+}) → Ca^{2+} + Al^{3+}. Furthermore, Fe^{3+} may partially substitute for Al (Holtstam, 1996). Terrestrial hibonite is usually brownish black to black in colour.

Kato and Saalfeld (1968) solved the crystal structure of synthetic hibonite confirming its isostructural relation to magnetoplumbite, $PbFe^{3+}_{12}O_{19}$. In hibonite, Ca has 12-fold coordination and Al ions are distributed over five independent crystallographic sites (Al1 to Al5), three octahedra (Al1, Al4 and Al5), one tetrahedron (Al3), and an unusual trigonal bipyramid (Al2) providing five-fold coordination by oxygen ions (Fig. 1). Al2 may be assigned to the 2*b* site on the mirror plane perpendicular to the *c* axis (central atom model). Alternatively, two half atoms may be placed at two equivalent 4*e* sites slightly shifted from the horizontal mirror plane (split atom model). Although the refinement of the central atom model allowing anharmonic thermal vibration for Al2 gave the same *R* value as the split atom model, the former gave larger peaks on difference Fourier maps than the latter (Utsunomiya *et al.*, 1988). Thus, the split atom model where Al2 occupies statistically one of two equivalent sites at the 4*e* positions (Fig. 1) seems to represent the correct structure model of hibonite at room temperature (Utsunomiya *et al.*, 1988). This ambiguity of dynamic properties of the atom at the bipyramidal site is a common problem in the magnetoplumbite-type structure (e.g. Kreber *et al.*, 1975; Obradors *et al.*, 1985; Utsunomiya *et al.*, 1988; Kimura *et al.*, 1990; Graetsch and Gebert, 1994; Bermanec *et al.*, 1996).

According to ^{57}Fe Mössbauer analyses of $BaFe_{12}O_{19}$ by Kreber *et al.* (1975), bipyramidal Fe jumps from one pseudo-tetrahedral site to the opposite one at high temperature, but it freezes at one of these positions below T = 80 K. Obradors *et al.* (1985) summarized three different models for the structural and dynamic characteristics of the bipyramidal sites: (1) an ordered configuration, (2) static disorder between two adjacent pseudo-tetrahedral sites, and (3) dynamic disorder between these sites. The result of the single-crystal analysis of $BaFe_{12}O_{19}$ at room temperature by Obradors *et al.* (1985) supported a disordered model interpreted as a fast diffusional motion within a quasiharmonic double-well potential.

Magnetoplumbite-related compounds are characterized by cubic (*c*) and hexagonal (*h*) closest-packed oxygen layers parallel to (001). The oxygen stacking sequence uses the symbols '*c*' and '*h*' where '*c*' indicates that a specific oxygen layer has neighbouring layers stacked in the cubic closest-packed fashion (ABC). Correspondingly, '*h*' stands for a layer where the layers above and below are of the same stacking type (e.g. the sequence is BCB or BAB).

A sequence of two cubic, closest-packed layers ('*cc*') represents the spinel module (or *S*-block) with small cations (*Y*) distributed at octahedrally and tetrahedrally coordinated sites. The composition of the spinel module, *S*-block, is Y_6O_8. A sequence of three hexagonal closest-packed layers ('*hhh*') is referred to as a conductor layer (Iyi *et al.*, 1989) or *R*-block (Kohn and Eckart, 1964). The central of the three hexagonal closest-packed oxygen layers has three instead of four oxygen atoms, because one is replaced by a large cation (*A*). Furthermore, the *R*-block hosts cations (*Y*) that are situated at octahedrally coordinated sites between the oxygen layers and in between three oxygen atoms of the central oxygen layer, resulting in trigonal-bipyramidal coordination. The composition of the *R*-block is AY_6O_{11}. The spinel module (*S*-block) and the conductor layer

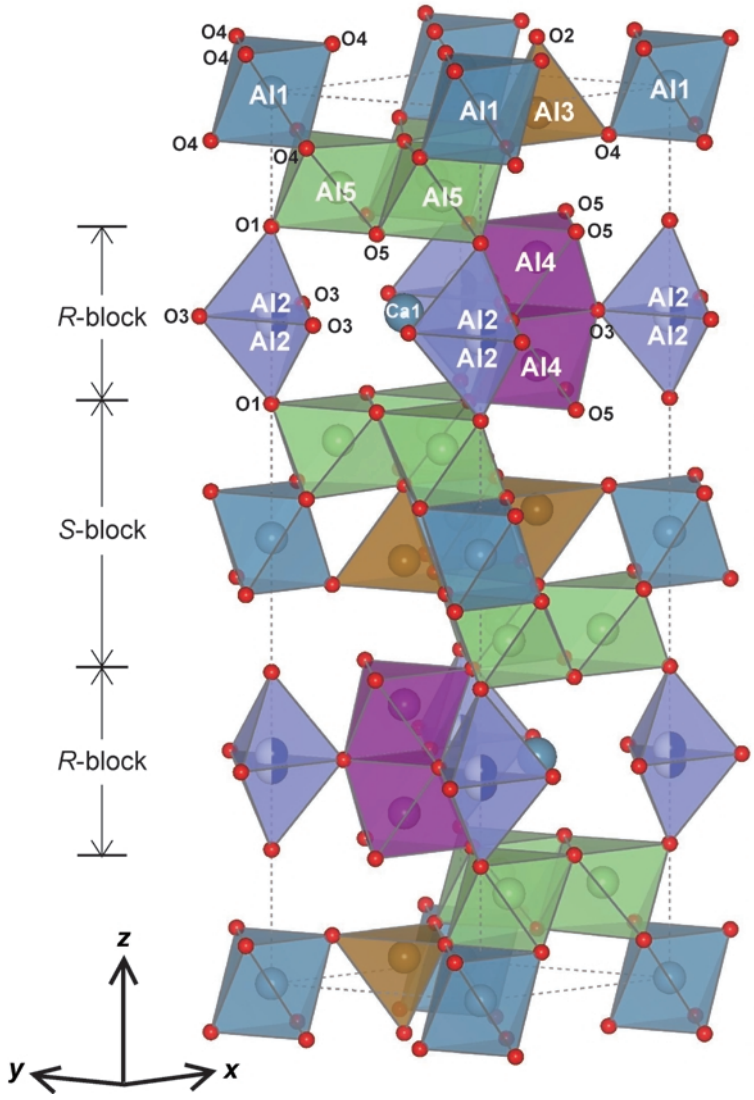

FIG. 1. Polyhedral representation of the hibonite structure drawn with the program *VESTA* (Momma and Izumi, 2008). Ca1, represented as a sphere, is twelve-fold coordinated by $6 \times$ O3 at the same height along **c** and $3 \times$ O5 above and below along **c**.

(*R*-block) can be stacked in different ratios. For magnetoplumbite and also hibonite, the *S*- and *R*-blocks alternate, hence the formula for *RS* is $AY_6O_{11} \cdot Y_6O_8 = AY_{12}O_{19}$. In magnetoplumbite-related structures the length of *a* is ~5.6 Å whereas the length of *c* depends on the stacking sequence.

Magnetoplumbite-type compounds are versatile in terms of technological application (Collongues *et al.*, 1990). They are used as permanent magnets known as 'hexagonal ferrites' in order to distinguish them from cubic ferromagnetic oxides with spinel or garnet structure. They are also used as catalyst supports in very high-temperature applications. Hibonite withstands significant radioactive radiation without metamictization and is therefore used in radioactive waste-immobilization technologies (Collongues *et al.*,

1990). Rare earth element (*REE*)-substituted synthetic hibonites are applied as luminescent or laser materials. $LaMgAl_{11}O_{19}$ is the best known of this family of materials known as LMA (Collongues *et al.*, 1990).

The precise structural characterization of natural hibonite establishes understanding of the complex substitution mechanisms occurring at the various Al sites. Although hibonite is the one of the simplest compounds in this group, its structural and dynamic properties have not yet been studied in an extended temperature range. In addition, this structure type has various high-temperature applications. The present paper examines the crystal structure of *REE*-free hibonite from an unspecified locality (probably Mogok) in Myanmar between 100 and 923 K using single-crystal X-ray diffraction (XRD).

Experimental methods

Material studied

A light yellow-orange-brown gem-bearing fragment (~3 mm × 3 mm × 5 mm) of hibonite from Myanmar (probably from the gemstone mines at Mogok) was made available to the authors for study. The crystal showed xenomorphic inclusions (up to 1 mm in maximum dimension) of corundum (confirmed by energy dispersive spectra (EDS) collected with a scanning electron microscope). In addition, the crystal showed oriented fractures and healing fissure-like features. Details of the specimen studied were given by Hainschwang *et al.* (2010).

Chemical analysis (EMPA)

The chemical composition of hibonite was determined using a JEOL JXA-8200 electron probe microanalyzer at the University of Bern. The abundances of Si, Ti, Al, Fe, Mn, Mg, Ca, Na, K and Zn were measured using an accelerating voltage of 15 kV and a beam current of 20 nA, with a beam diameter of 10 μm. The following reference materials were used: wollastonite (Si-*K*α, TAP; Ca-*K*α, PET), synthetic ilmenite (Ti-*K*α, PET; Fe-*K*α, LIF), synthetic spinel (Al-*K*α, TAP; Mg-*K*α, TAP), synthetic tephroite (Mn-*K*α, LIF), albite (Na-*K*α, TAP), orthoclase (K-*K*α, PET), and synthetic gahnite (Zn-*K*α, LIF). The PRZ method (modified ZAF) with $\phi(\rho Z)$ integration for the atomic number correction (Packwood and Brown, 1981; Bastin *et al.*, 1984, 1986) was used for data correction.

Single-crystal structure analysis

X-ray diffraction data for a single crystal of hibonite were collected using a Bruker SMART APEX II CCD diffractometer. The transparent orange crystal was mounted on a glass fibre for room-temperature measurement and subsequently loaded into a 0.1 mm diameter quartz-glass capillary tube for low- to high-temperature measurements. The lattice parameters were determined at temperatures of 100, 150, 200, 250, 300, 350, 400, 450, 473, 523, 573, 623, 673, 723, 773, 823, 873 and 923 K using twelve sets of frames. Intensity data were measured at 100 K, 296 K (room temperature), 473 K and 923 K using graphite-monochromatized Mo-*K*α radiation (λ = 0.71069 Å). The crystal was cooled by means of a nitrogen stream allowing temperatures as low as 100 K. Subsequently, the crystal was heated using a self-constructed, regulated, hot N_2 blower, calibrated at several phase transitions, monitored by the corresponding diffraction patterns. Preliminary lattice parameters and an orientation matrix were obtained from twelve sets of frames and refined during the integration process of the intensity data. Diffraction data were collected with ω scans at different φ settings (φ-ω scan) (Bruker, 1999). The data were processed using *SAINT* (Bruker, 1999). An empirical absorption correction using *SADABS* (Sheldrick, 1996) was applied. The reflection statistics and systematic absences were consistent with space group $P6_3/mmc$. Structural refinement was performed using *SHELXL*-97 (Sheldrick, 2008). Scattering factors for neutral atoms were employed. The site occupancies for the Ca1, Al1, Al2, Al3, Al4 and Al5 sites were refined in the data set of room-temperature measurements, and the values were fixed in the data set measured at 100, 473 and 923 K during the refinements. Atomic displacement parameters were analysed applying the program *THMA11* (Trueblood, 1978) within the *WinGX* suite (Farrugia, 1999) and displayed using *PEANUT* (Hummel *et al.*, 1990). Bond-valence sums of the structures at 100 K and 923 K were calculated using the electrostatic strength function of Brown and Altermatt (1985) and the bond-valence parameters of Brese and O'Keeffe (1991).

Results

Chemical composition of hibonite

The average chemical composition of the hibonite sample, based on 21 point analyses, is given in

TABLE 1. Composition of hibonite based on 21 point analyses.

Oxide	wt.%	s.d.	Element	a.p.f.u.*	s.d.
SiO_2	0.74	0.02	Si	0.08	<0.01
TiO_2	6.11	0.13	Ti	0.52	0.01
Al_2O_3	80.62	0.32	Al	10.74	0.02
FeO**	0.41	0.07	Fe^{2+}	0.04	0.01
MgO	3.05	0.07	Mg	0.51	0.01
CaO	8.19	0.06	Ca	0.99	0.01
Na_2O	0.04	0.01	Na	0.01	<0.01
ZnO	1.28	0.15	Zn	0.11	0.01
Total	100.44		Total	13.00	

* Total cations = 13
** Total Fe as FeO

Table 1, where total Fe is reported as FeO. The corresponding crystal chemical formula is $(Ca_{0.99}Na_{0.01})_{\Sigma 1.00}(Al_{10.74}Ti_{0.52}Mg_{0.51}Zn_{0.11}Si_{0.08}Fe^{2+}_{0.04})_{\Sigma 12.00}O_{18.97}$ with the number of cations normalized to 13, and O calculated using charge-balance considerations. Although hibonite samples from terrestrial environments, *i.e.* Madagascar (Curien *et al.*, 1956; Maaskant *et al.*, 1980; Bermanec *et al.*, 1996), Tanzania (Maaskant *et al.*, 1980) and India (Santosh *et al.*, 1991) often contain *REE*, REE_2O_3 was not detected in the sample in the present study. The crystal analysed was subsequently used for the single-crystal XRD experiment.

Crystal-structure solution and refinement

The crystallographic data and refinement parameters are summarized in Table 2. The refined atomic positions and anisotropic displacement parameters are listed in Tables 3 and 4, respectively. The crystal structure of hibonite is shown in Fig. 1. Table 5 summarizes site occupancies for hibonite. According to the refined site-scattering values, site occupancies at Ca1, Al1 and Al5 were fixed as fully occupied by Ca (Ca1) and Al (Al1 and Al5) in the final refinement. The maximum site occupancy of the trigonal bipyramid Al2 site is 1/2 because the 4*e* site is slightly shifted from the (001) mirror plane. Selected interatomic distances are presented in Table 6. Results of bond-valence calculations are given in Table 7. The unit-cell parameters measured at different temperatures are listed in Table 8.

Discussion

The crystal structure of natural hibonite with complex cation substitution (Bermanec *et al.*, 1996; this study) may be compared with one of synthetic end-members (Utsunomiya *et al.*, 1988). At ambient conditions, there are several striking differences between the natural and the synthetic samples: (1) the unit-cell volume of synthetic $CaAl_{12}O_{19}$ of 585.83(1) Å^3 is 1.6% smaller than that of the mineral; (2) the atomic displacement parameters evaluated as U_{eq} of most atomic sites of the natural sample are ~1.8 times larger than those of $CaAl_{12}O_{19}$. The U_{eq} values of Al2 and Al3 of the mineral are more than twice as large as those of $CaAl_{12}O_{19}$; and (3) there are significant differences between corresponding bond lengths of the natural and the synthetic samples.

Site-occupancy refinements indicate that the Ti in the mineral is distributed between Al2 and Al4, while the tetrahedral site, Al3, contains minor amounts of Zn. The similar X-ray scattering power of Al and Mg makes a straightforward assignment of Mg difficult. The data available enable us to make certain predictions. The Fe concentration in hibonite from Myanmar (0.41 wt.% FeO) is too small to be differentiated from Ti (6.11 wt.% TiO_2) by XRD.

Octahedrally coordinated Al1 site

Compared to synthetic $CaAl_{12}O_{19}$ (Utsunomiya *et al.*, 1988), the six bond lengths for Al1–O4 of hibonite from Myanmar (this study) and Madagascar (Bermanec *et al.* 1996) are only 0.004 Å longer. Thus, in accordance with the

TABLE 2. Experimental details of the single-crystal XRD analysis of hibonite*.

Temperature (K)		100	296	473	923
Crystal size (mm)		$0.1 \times 0.07 \times 0.025$			
Space group		$P6_3/mmc$			
Cell parameters	a (Å)	5.5901(1)	5.5909(1)	5.6001(1)	5.6178(1)
	c (Å)	21.9710(4)	21.9893(4)	22.0291(4)	22.1446(3)
	V (Å^3)	594.59	595.26	598.30	605.24
Dcalc (g/cm^3)		3.813	3.809	3.789	3.746
Radiation		Mo-$K\alpha$ (λ = 0.71069 Å)			
Monochromator		Graphite			
Diffractometer		Bruker APEX CCD			
Scan type		φ-ω scan (Bruker, 1999)			
Absorption correction		SADABS (Sheldrick, 1996)			
θ_{min} (°)		1.9	1.9	1.9	1.8
θ_{max} (°)		34.5	34.6	34.3	34.3
μ (mm^{-1})		1.340	1.338	1.331	1.316
Collected reflections		7810	8751	17527	9021
Unique reflections		540	543	538	545
R_{int} (%)		3.88	3.53	4.38	3.88
R_σ (%)		1.81	1.50	1.30	1.85
Miller index limits	h	$-8 \rightarrow 8$	$-8 \rightarrow 8$	$-8 \rightarrow 8$	$-8 \rightarrow 8$
	k	$-8 \rightarrow 8$	$-8 \rightarrow 8$	$-8 \rightarrow 8$	$-6 \rightarrow 8$
	l	$-35 \rightarrow 28$	$-32 \rightarrow 34$	$-34 \rightarrow 34$	$-34 \rightarrow 29$
Refinement on F^2 using		*SHELXL*-97 (Sheldrick, 2008)			
R_1 (%)		2.09	1.86	2.08	2.46
wR_2 (%)		6.55	6.44	6.55	7.66
No. of parameters		43	46	43	43
Weighting scheme**		$w = 1/[s^2(F_o^2) + (0.0376P)^2]$	$w = 1/[s^2(F_o^2) + (0.0375P)^2 + 0.09P]$	$w = 1/[s^2(F_o^2) + (0.0433P)^2]$	$w = 1/[s^2(F_o^2) + (0.0437P)^2 + 0.01P]$
Extinction		0.0081	0.0041	0.0086	0.0073
$\Delta\rho_{max}$ (e Å^{-3})		0.356 at 0.17 Å from O2	0.367 at 0.67 Å from O2	0.377 at 0.51 Å from O3	0.366 at 0.51 Å from O5
$\Delta\rho_{min}$ (e Å^{-3})		−0.559 at 0.13 Å from Al3	−0.302 at 0.43 Å from Al4	−0.542 at 0.14 Å from Al3	−0.416 at 0.14 Å from Al1

* Chemical formula is represented as $(Ca_{0.99}Na_{0.01})_{\Sigma 1.00}(Al_{10.74}Ti_{0.52}Mg_{0.51}Zn_{0.11}Si_{0.08}Fe^{2+}_{0.04})_{\Sigma 12.00}O_{18.97}$ (Z = 2).
** The function of the weighting scheme is $w = 1/(s^2(F_o^2) + (a \cdot P)^2 + b \cdot P)$, where $P = (\mathrm{Max}(F_o^2)+2F_c^2)/3$, and the parameters a and b are chosen to minimize the differences in the variances for reflections in different ranges of intensity and diffraction angle.

observed scattering power, Al1 is assumed to be a pure Al site.

Al2 (half-occupied, distorted tetrahedral or fully occupied, trigonal bibyramidal coordination)

For synthetic $CaAl_{12}O_{19}$, Utsunomiya *et al.* (1988) addressed the problem of whether Al at Al2 is in trigonal bipyramidal coordination undergoing anharmonic vibration (anharomic terms up to the fourth order), or in distorted tetrahedral coordination (split atom model). Their experimental data clearly favoured the split-atom model. However, at room temperature, we are undecided between two possible interpretations: (1) statistical disorder of two 50% occupied subsites; or (2) dynamic transposition between the two sites. In contrast, Abrahams *et al.* (1987), studying isotypic $LaMgAl_{11}O_{19}$, preferred the anharmonic model for Al2, using coefficients to the fifth rank, with Al in trigonal bipyramidal coordination.

For hibonite from Myanmar the interpretation is even more difficult because Al on Al2 is

TABLE 3. Atomic positions and equivalent displacement parameters (Å^2).

Site	W*		100 K	296 K	473 K	923 K
Ca1	2*d*	*x*	⅔	⅔	⅔	⅔
		y	⅓	⅓	⅓	⅓
		z	¼	¼	¼	¼
		*U*eq	0.0160(2)	0.0221(2)	0.0274(2)	0.0423(3)
Al1	2*a*	*x*	0	0	0	0
		y	0	0	0	0
		z	0	0	0	0
		*U*eq	0.0035(2)	0.0056(2)	0.0066(2)	0.0118(3)
Al2	4*e*	*x*	0	0	0	0
		y	0	0	0	0
		z	0.7421(2)	0.7428(4)	0.7421(3)	0.7408(2)
		*U*eq	0.0102(9)	0.014(1)	0.0143(9)	0.019(1)
Al3	4*f*	*x*	⅓	⅓	⅓	⅓
		y	⅔	⅔	⅔	⅔
		z	0.02761(3)	0.02759(3)	0.02761(3)	0.02753(4)
		*U*eq	0.0047(2)	0.0066(2)	0.0079(2)	0.0139(2)
Al4	4*f*	*x*	⅔	⅔	⅔	⅔
		y	⅓	⅓	⅓	⅓
		z	−0.18924(3)	−0.18918(3)	−0.18910(3)	−0.18894(3)
		*U*eq	0.0039(2)	0.0058(2)	0.0071(2)	0.0128(2)
Al5	12*k*	*x*	0.16785(4)	0.16793(4)	0.16788(3)	0.16797(5)
		y	0.33569(8)	0.33586(7)	0.33575(7)	0.33595(9)
		z	−0.10808(2)	−0.10802(2)	−0.10798(2)	−0.10789(2)
		*U*eq	0.0041(1)	0.0058(1)	0.0070(1)	0.0127(2)
O1	4*e*	*x*	0	0	0	0
		y	0	0	0	0
		z	0.84939(8)	0.84950(7)	0.84951(7)	0.8499(1)
		*U*eq	0.0063(3)	0.0071(3)	0.0080(3)	0.0136(4)
O2	4*f*	*x*	⅓	⅓	⅓	⅓
		y	⅔	⅔	⅔	⅔
		z	−0.05740(8)	−0.05724(7)	−0.05734(7)	−0.05731(9)
		*U*eq	0.0053(3)	0.0068(3)	0.0083(3)	0.0146(4)
O3	6*h*	*x*	−0.1807(1)	−0.1803(1)	−0.1803(1)	−0.1800(2)
		y	0.1807(1)	0.1803(1)	0.1803(1)	0.1800(2)
		z	3/4	3/4	3/4	3/4
		*U*eq	0.0068(3)	0.0096(3)	0.0118(3)	0.0196(4)
O4	12*k*	*x*	0.1524(1)	0.15255(9)	0.15255(8)	0.1527(1)
		y	0.3049(2)	0.3051(2)	0.3051(2)	0.3055(2)
		z	0.05316(5)	0.05313(4)	0.05305(4)	0.05294(6)
		*U*eq	0.0067(2)	0.0084(2)	0.0097(2)	0.0150(3)
O5	12*k*	*x*	0.50425(8)	0.50399(7)	0.50406(6)	0.50375(9)
		y	0.49575(8)	0.49601(7)	0.49594(6)	0.49625(9)
		z	0.34998(4)	0.35007(4)	0.35013(4)	0.35035(6)
		*U*eq	0.0048(2)	0.00650(19)	0.0081(2)	0.0146(3)

* W = Wykoff notation of point position

partially replaced by ~17% Ti. Our refinement indicated two half-occupied subsites only 0.32 Å apart (0.33 Å in synthetic $CaAl_{12}O_{19}$). However, the mean-square displacement value for Al2 of our sample parallel to *c* (U_{33}), the direction of site splitting, is three times as large as the corresponding value in synthetic $CaAl_{12}O_{19}$. The increased U_{33} is interpreted due to disorder of ions of different size (Al, Ti) within a strongly distorted tetrahedron. In contrast to $U_{11} = U_{22}$,

TABLE 4. Anisotropic displacement parameters (Å^2).

Site		100 K	296 K	473 K	923 K
Ca1	U_{11}	0.0173(3)	0.0228(3)	0.0279(3)	0.0417(5)
	U_{22}	0.0173(3)	0.0228(3)	0.0279(3)	0.0417(5)
	U_{33}	0.0135(4)	0.0207(4)	0.0263(5)	0.0435(7)
	U_{23}	0	0	0	0
	U_{13}	0	0	0	0
	U_{12}	0.0086(1)	0.0114(1)	0.0140(1)	0.0209(2)
Al1	U_{11}	0.0033(3)	0.0050(2)	0.0066(3)	0.0122(4)
	U_{22}	0.0033(3)	0.0050(2)	0.0066(3)	0.0122(4)
	U_{33}	0.0039(4)	0.0067(4)	0.0066(4)	0.0110(6)
	U_{23}	0	0	0	0
	U_{13}	0	0	0	0
	U_{12}	0.0017(1)	0.0025(1)	0.0033(1)	0.0061(2)
Al2	U_{11}	0.0035(3)	0.0049(3)	0.0062(3)	0.0117(4)
	U_{22}	0.0035(3)	0.0049(3)	0.0062(3)	0.0117(4)
	U_{33}	0.024(3)	0.033(4)	0.031(3)	0.034(3)
	U_{23}	0	0	0	0
	U_{13}	0	0	0	0
	U_{12}	0.0017(2)	0.0025(2)	0.0031(1)	0.0058(2)
Al3	U_{11}	0.0043(2)	0.0060(2)	0.0074(2)	0.0130(3)
	U_{22}	0.0043(2)	0.0060(2)	0.0074(2)	0.0130(3)
	U_{33}	0.0055(3)	0.0079(3)	0.0087(3)	0.0156(4)
	U_{23}	0	0	0	0
	U_{13}	0	0	0	0
	U_{12}	0.0022(1)	0.0030(1)	0.0037(1)	0.0065(1)
Al4	U_{11}	0.0037(2)	0.0058(2)	0.0073(2)	0.0133(3)
	U_{22}	0.0037(2)	0.0058(2)	0.0073(2)	0.0133(3)
	U_{33}	0.0043(3)	0.0056(3)	0.0068(3)	0.0119(4)
	U_{23}	0	0	0	0
	U_{13}	0	0	0	0
	U_{12}	0.0018(1)	0.0029(1)	0.00364(9)	0.0066(1)
Al5	U_{11}	0.0038(2)	0.0054(2)	0.0066(2)	0.0121(2)
	U_{22}	0.0037(2)	0.0049(2)	0.0061(2)	0.0107(3)
	U_{33}	0.0048(2)	0.0069(2)	0.0082(2)	0.0149(3)
	U_{23}	0.0001(1)	0.0001(1)	0.0003(1)	0.0006(2)
	U_{13}	0.00002(6)	0.00002(5)	0.00013(5)	0.00029(8)
	U_{12}	0.0018(1)	0.00247(9)	0.0030(1)	0.0054(1)
O1	U_{11}	0.0052(5)	0.0056(4)	0.0071(4)	0.0114(6)
	U_{22}	0.0052(5)	0.0056(4)	0.0071(4)	0.0114(6)
	U_{33}	0.0084(7)	0.0101(7)	0.0100(7)	0.0181(9)
	U_{23}	0	0	0	0
	U_{13}	0	0	0	0
	U_{12}	0.0026(3)	0.0028(2)	0.0035(2)	0.0057(3)
O2	U_{11}	0.0041(4)	0.0055(4)	0.0076(4)	0.0136(6)
	U_{22}	0.0041(4)	0.0055(4)	0.0076(4)	0.0136(6)
	U_{33}	0.0076(8)	0.0095(7)	0.0098(7)	0.017(1)
	U_{23}	0	0	0	0
	U_{13}	0	0	0	0
	U_{12}	0.0020(2)	0.0027(2)	0.0038(2)	0.0068(3)
O3	U_{11}	0.0068(5)	0.0111(4)	0.0144(5)	0.0253(8)
	U_{22}	0.0068(5)	0.0111(4)	0.0144(5)	0.0253(8)
	U_{33}	0.0063(6)	0.0080(6)	0.0096(6)	0.0150(8)
	U_{23}	0	0	0	0
	U_{13}	0	0	0	0
	U_{12}	0.0031(5)	0.0066(5)	0.0095(5)	0.0177(8)

Table 4 (*contd.*)

Site		100 K	296 K	473 K	923 K
O4	U_{11}	0.0057(3)	0.0076(3)	0.0091(3)	0.0152(5)
	U_{22}	0.0084(5)	0.0107(4)	0.0112(4)	0.0162(6)
	U_{33}	0.0067(5)	0.0078(4)	0.0094(4)	0.0141(6)
	U_{23}	−0.0024(3)	−0.0022(3)	−0.0024(3)	−0.0024(4)
	U_{13}	−0.0012(2)	−0.0011(1)	−0.0012(2)	−0.0012(2)
	U_{12}	0.0042(2)	0.0054(2)	0.0056(2)	0.0081(3)
O5	U_{11}	0.0043(3)	0.0055(3)	0.0070(3)	0.0125(4)
	U_{22}	0.0043(3)	0.0055(3)	0.0070(3)	0.0125(4)
	U_{33}	0.0056(4)	0.0081(4)	0.0098(4)	0.0174(6)
	U_{23}	0.0000(2)	0.0006(1)	0.0010(1)	0.0024(2)
	U_{13}	−0.0000(2)	−0.0006(1)	−0.0010(1)	−0.0024(2)
	U_{12}	0.0020(4)	0.0024(3)	0.0030(3)	0.0051(5)

which, between temperatures of 100 and 923 K, increased by a factor of three, U_{33} increased by a factor of 1.4 but lacks significant temperature dependence between 296 and 923 K. The small increase in U_{33} with increasing temperature supports a static disorder model (Fig. 2).

As seen in Fig. 1 the distances O1−O1 (Table 5) along the *c* axis may be used to evaluate the thermal expansion of the *R*- and the *S*-block, respectively. The variation in $(O1-O1)/(O1-O1)_0$ with temperature is shown in Fig. 3 (reference 100 K). The expansion of the *R*-block including the Al2 site is steeper than that of the *S*-block.

Tetrahedrally coordinated Al3

In synthetic $CaAl_{12}O_{19}$ (Utsunomiya *et al.*, 1988) Al3−O2 (1 ×) and Al3−O4 (3 ×) distances are 1.810 and 1.796 Å, respectively. Both the Myanmar (this study) and the Madagascar (Bermanec *et al.*, 1996) samples show distances increased by 0.055 and 0.043 Å, respectively. In the refinement of the Myanmar sample, we located ~5% Zn substitution for Al but this value cannot explain the significant size difference between the tetrahedra of the synthetic and the Myanmar crystals. If we assume a Mg−O distance for tetrahedral coordination of 1.96 Å (Shannon, 1976), the enlarged Al3 tetrahedron of the Myanmar hibonite contains ~70% Al, 5% Zn, and 25% Mg. 25% Mg at Al3 corresponds to 0.5 Mg per formula unit (p.f.u.). Thus, all Mg analysed is assumed to be in tetrahedral coordination. Assignment of Mg to this tetrahedral site is also verified by the isotypic structure of $LaMgAl_{11}O_{19}$ where Mg occupies, together with Al (1:1 ratio), a corresponding position (Abrahams *et al.*, 1987). An additional indicator for the preference of Mg being present at the Al3 site is the bond valence (Table 7), which is ~2.2 valence units (v.u.) for hibonite from Myanmar (assuming 95% Al and 5% Zn at Al3) but 2.5 v.u. for synthetic $CaAl_{12}O_{19}$ (Utsunomiya *et al.*, 1988).

TABLE 5. Site occupancies of hibonite.

Site	Site occupancy
Ca1	Ca1.0
Al1	Al1.0
Al2	Al0.413(4),Ti0.087(4)
Al3	Al*0.955(2),Zn0.045(2)
Al4	Al0.778(5),Ti0.222(5)
Al5	Al1.0

* Refined Al occupancy at Al3 includes 0.5 Mg.

The ubiquitous SiO_2 (up to 3 wt.% corresponding to 0.3 Si p.f.u.) analysed in all natural hibonites (Table 1) remains enigmatic. The dense cation distribution in hibonite does not allow for interstitial sites without close contacts with other occupied polyhedra. Thus, Si is probably incorporated into the large Al3 tetrahedra (~4% Si substitution corresponding to 0.74 wt.% SiO_2 analysed for the Myanmar sample).

Substitution of large (Mg, Zn) and small (Si) cations for tetrahedral Al is expected to cause substantial static disorder, which may be analysed by difference mean square displacement amplitudes ($\Delta(U_O-U_{Al3})$) along the bonding vector (Kunz and Armbruster, 1990). For synthetic $CaAl_{12}O_{19}$, $<\Delta(U_O-U_{Al3})>$ is −0.0001(2) but

TABLE 6. Selected interatomic distances (Å).

		100 K	296 K	473 K	923 K
Ca1 −O3	×6	2.7984(5)	2.7986(5)	2.8032(5)	2.8119(5)
−O5	×6	2.7016(9)	2.7062(9)	2.7117(9)	2.730(1)
Mean		2.7500	2.7524	2.7575	2.771
Al1 −O4	×6	1.882(1)	1.8834(9)	1.8855(9)	1.893(1)
Al2 −O1		2.011(6)	2.029(8)	2.019(6)	2.008(5)
−O3	×3	1.759(1)	1.753(1)	1.758(1)	1.763(2)
Mean		1.822	1.822	1.823	1.824
Al3 −O2		1.868(2)	1.865(2)	1.871(2)	1.879(2)
−O4	×3	1.839(1)	1.8386(9)	1.8408(8)	1.845(1)
Mean		1.846	1.845	1.848	1.854
Al4 −O3	×3	1.991(1)	1.996(1)	2.0005(9)	2.014(1)
−O5	×3	1.8658(9)	1.8643(8)	1.8680(7)	1.873(1)
Mean		1.928	1.930	1.9343	1.944
Al5 −O1		1.8746(9)	1.8754(9)	1.8783(8)	1.883(1)
−O2		1.951(1)	1.9525(9)	1.9545(9)	1.961(1)
−O4	×2	1.9690(8)	1.9700(7)	1.9738(7)	1.9828(9)
−O5	×2	1.8356(6)	1.8367(6)	1.8394(6)	1.8457(8)
Mean		1.9058	1.9069	1.9099	1.9168
O1−O1 (*R*-block)		4.367(2)	4.376(2)	4.384(2)	4.423(3)
O1−O1 (*S*-block)		6.618(2)	6.619(2)	6.630(2)	6.649(3)

becomes 0.0043(5) for Myanmar hibonite at room temperature. At 100 K, disorder-related smearing of oxygen along the Al3−O vector could be visualized. At higher temperature, this effect remains but is masked by additional thermal motion. The versatile occupation of Al3 is also responsible for its above-average displacement parameter.

TABLE 7. Bond-valence sum of hibonite (v.u.).

Site	100 K	296 K	923 K
Ca1	1.51	1.50	1.43
Al1	2.96	2.94	2.87
Al2	2.64	2.66	2.62
Al3*	2.19	2.20	2.15
Al4	2.90	2.89	2.79
Al5	2.81	2.80	2.73
O1	1.89	1.87	1.86
O2	1.74	1.74	1.70
O3	1.78	1.78	1.71
O4	1.83	1.83	1.78
O5	1.82	1.82	1.77

*Calculated for 0.95 Al + 0.05 Zn

TABLE 8. Variations in the unit-cell parameters of hibonite between 100 K and 923 K.

Temp. (K)	*a* (Å)	*c* (Å)	*V* (Å^3)
100	5.5901(1)	21.9710(4)	594.59(1)
150	5.5903(7)	21.988(4)	595.10(6)
200	5.5914(5)	21.983(3)	595.20(6)
250	5.5922(7)	21.991(4)	595.58(5)
300	5.5930(5)	22.000(3)	596.01(6)
350	5.5945(5)	22.005(3)	596.44(6)
400	5.5958(4)	22.011(3)	596.88(6)
450	5.5984(4)	22.023(3)	597.77(6)
473	5.5997(4)	22.031(3)	598.28(4)
523	5.6017(4)	22.046(2)	599.09(4)
573	5.6038(4)	22.059(2)	599.91(5)
623	5.6061(4)	22.071(2)	600.71(5)
673	5.6081(4)	22.083(3)	601.47(5)
723	5.6109(3)	22.093(2)	602.37(5)
773	5.6131(3)	22.106(2)	603.18(5)
823	5.6160(3)	22.121(2)	604.23(5)
873	5.6186(3)	22.134(2)	605.12(5)
923	5.6207(3)	22.148(2)	605.96(5)

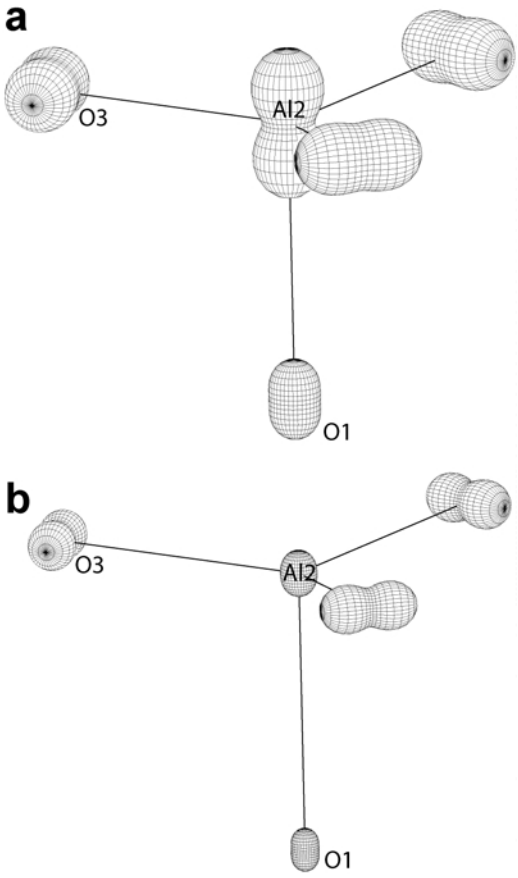

FIG. 2. *PEANUT* drawing (Hummel *et al.*, 1990) of the distorted tetrahedrally coordinated Al2 site in hibonite: (*a*) representing mean-square displacement parameters measured at 923 K (scale $\times 16$); (*b*) representing difference mean-square displacement parameters evaluated between 100 and 923 K (scale $\times 16$). The large anisotropic 'peanut' around Al2 at 923 K (*a*) indicates positional disorder. The small 'peanut' around Al2 in the difference plot (*b*) excludes dynamic (temperature-dependent, time-averaged) disorder but suggests dominant static (space-averaged) disorder (Ti, Al).

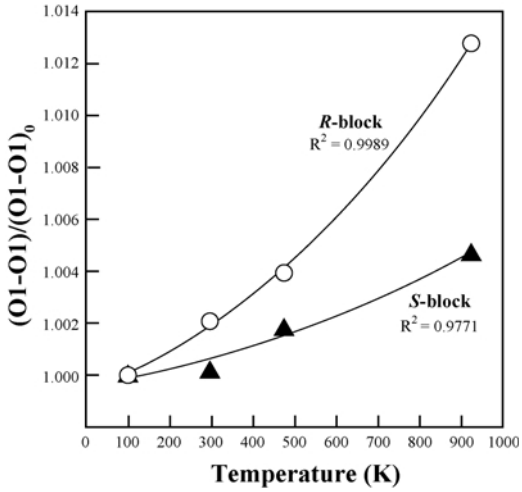

FIG. 3. Variation of $(O1-O1)/(O1-O1)_0$ with temperature. Open circles represent the O1–O1 distance for the *R*-block; closed triangles that for the *S*-block; the reference is the value measured at 100 K.

Octahedrally coordinated Al4

For hibonite from Myanmar, we refined 22% Ti replacing Al at Al4. As a consequence <Al4–O> is 0.03 Å longer than for synthetic $CaAl_{12}O_{19}$ (Utsunomiya *et al.*, 1988). The influence of Ti substitution on octahedral bond-length distortion is even more striking. For synthetic $CaAl_{12}O_{19}$, the difference between Al4–O3 and Al4–O5 is 0.078 Å, but the difference increases to 0.132 Å for Myanmar hibonite. This can be understood by considering that adjacent Al4 octahedra share faces parallel to (001) and three O3 type oxygen atoms form the common triangular face. For electrostatic reasons (repulsion), cations in the Al4 octahedron favour an out-of-centre position, which increases Al4–O3 and decreases Al4–O5 with increasing cation charge.

Octahedrally coordinated Al5

Hibonite from Madagascar (Bermanec *et al.*, 1996) and Myanmar (this study) have no heavy elements at Al5. This position seems to be a pure Al site. In synthetic $CaAl_{12}O_{19}$ (Utsunomiya *et al.*, 1988), the difference between the longest Al5–O distance (Al5–O4) and the shortest distance (Al5–O5) is 0.193 Å. The Al5 octahedron in Myanmar hibonite is less distorted in terms of bond lengths and the maximum difference is only 0.133 Å. This is also confirmed by the bond-length distortion parameter of Al5 defined by Baur (1974), which is 0.030 for Myanmar hibonite but 0.046 for the synthetic analogue. In fact, Al5–O4 in the mineral is shorter but Al5–O5 is longer than corresponding distances in the synthetic analogue. O4 and O5 also contribute to tetrahedral Al3 and the face-sharing dimers of octahedra (Al4). Thus, substitutions on the latter sites have a balancing effect on the distortion of the Al5 octahedron.

Twelve-coordinated Ca1

Ca1 replaces oxygen in a closest-packed layer formed by O3. Bond-valence calculations (Table 7) indicate that Ca is underbonded (1.5 v.u.). In line with this finding is a 'rattling-type' motion (Armbruster and Geiger, 1993) of Ca within a rather rigid oxygen coordination-polyhedron (Fig. 4). Within (001), Ca is bonded 6× to O3 and also below and above this plane 6× to O5. The rattling motion can be visualized by displaying difference mean-square displacement parameters evaluated at the extreme temperatures 100 and 923 K (Δ = 823 K). This plot (Fig. 4) shows a stronger motion for Ca than for the coordinating light oxygen atoms.

Thermal expansion between 100 and 923 K (Δ = 823 K)

Hazen and Prewitt (1977) derived the empirical relationship for bond expansion:

$<\alpha>$ (10^{-6} K^{-1}) = 32.9 (0.75−z/ρ), where z is the cation charge and ρ the coordination number. If we apply this simple relationship to octahedral and tetrahedral Al, the following mean expansion coefficients are predicted: Al^{VI}: 8.2×10^{-6} K^{-1} and Al^{IV}: 0. For Ca^{XII} the formula predicts 19.2×10^{-6} K^{-1} and thus Ca−O extension is expected to be a dominant contributor to the bulk expansion of hibonite. In contrast, our structural data between 296 K and 923 K yield a Ca−O bond expansion of only 10.1×10^{-6} K^{-1}, almost half of the predicted value. The observed value is in line with the result derived previously, *i.e.* that Ca in hibonite is actually too small for the cuboctahedron of oxygen atoms about the Ca and it therefore engages in a 'rattling' motion. The measured values for the pure Al octahedra, Al1 and Al5 are 8.1 and 8.3×10^{-6} K^{-1} in excellent agreement with prediction. The Ti^{4+}-substituted octahedron, Al4 (11.6×10^{-6} K^{-1}) exceeds slightly the reference value as does the Al3 tetrahedron (7.8×10^{-6} K^{-1}), which has ~25% Mg. An expansion of 8.2×10^{-6} K^{-1} is predicted for a pure Mg tetrahedron.

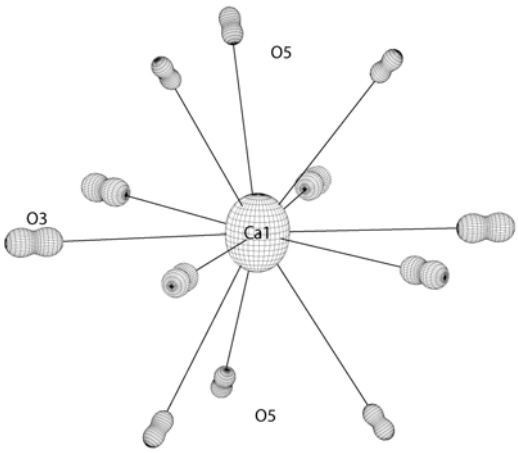

FIG. 4. *PEANUT* drawing (Hummel *et al.*, 1990) of the twelve-coordinated Ca1 site in hibonite, replacing O in a closest-packed ABC arrangement. Difference mean-square displacement parameters evaluated between 100 and 923 K (scale ×16) show a significantly larger 'vibrational smearing' for the central Ca compared to coordinating oxygen atoms. This is unusual because, normally, vibrational amplitudes are correlated with atomic weight. Therefore, Ca is interpreted as a 'rattling' ion within a outsized coordination 'box'.

The thermal expansion behaviour of hibonite (this study) is compared with the dilatometrical data between 295 and 860 K for $LaMgAl_{11}O_{19}$ (Abrahams *et al.*, 1987), isotypic with hibonite (Fig. 5). Myanmar hibonite and synthetic $LaMgAl_{11}O_{19}$ show very similar expansion properties, although the increase of cell dimensions and volume with temperature is slightly greater in the natural sample (Table 8). The following functions describe the temperature dependence (T in Kelvin) of cell dimensions for Myanmar hibonite: $a_T = 5.5930 + 3.47 \times 10^{-5} T + 1.67 \times 10^{-8} T^2$ ($R^2 = 0.9988$, reference 300 K) and $c_T = 22.000 + 1.75 \times 10^{-4} T + 1.05 \times 10^{-7} T^2$ ($R^2 = 0.9952$, reference 300 K). Between 296 and 923 K, the thermal expansion coefficients are $\alpha_a = 7.64 \times 10^{-6}$ K^{-1}, $\alpha_c = 11.19 \times 10^{-6}$ K^{-1}, and $\alpha_V = 26.30 \times 10^{-5}$ K^{-1}. The corresponding values for synthetic $CaAl_{12}O_{19}$ for the x and z axes are $\alpha_a = 7.3 \times 10^{-6}$ K^{-1} and $\alpha_c = 11.8 \times 10^{-6}$ K^{-1} (Sánchez-Herencia *et al.*, 2000). Due to the very small increase in Ca−O bond lengths with temperature in hibonite or synthetic hexaaluminate (CA_6), thermal expansion is similar to that of corundum (Aldebert and Traverse, 1984), classifying CA_6 ('Bonite') as an interesting refractory for versatile applications (Büchel *et al.*, 2005). In addition, CA_6 shows high-temperature stability, lower thermal conductivity and better alkali resistance than corundum (Büchel *et al.*, 2005; Kockegey-Lorenz *et al.*, 2005), which makes it even superior to corundum for specific insulating refractory applications.

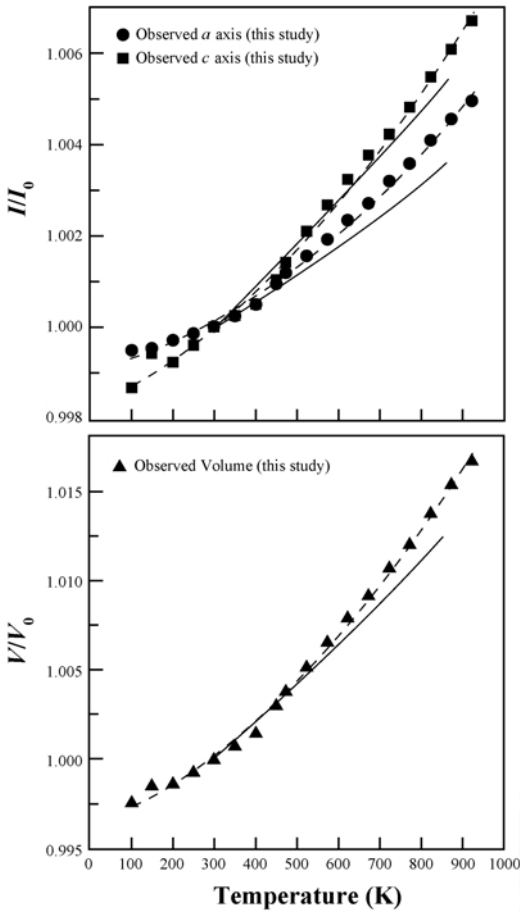

FIG. 5. Relative thermal expansion of Myanmar hibonite (triangular symbols connected by dashed lines) compared to iso-structural $LaMgAl_{11}O_{19}$ (Abrahams *et al.*, 1987) shown by solid lines.

Acknowledgements

The authors are grateful to M. Welch, Principal Editor, and to S.J. Mills, F. Cámara, C. Ma and D. Gatta for their constructive comments.

References

Abrahams, S.C., Marsh, P. and Brandle, C.D. (1987) Laser and phosphor host $La_{1-x}MgAl_{11+x}O_{19}$ (x = 0.050): Crystal structure at 295 K. *Journal of Chemical Physics*, **86**, 4221–4227.

Aldebert, P. and Traverse, J.P. (1984) α-Al_2O_3, a high-temperature thermal expansion standard. *High Temperatures High Pressures*, **16**, 127–135.

Armbruster, T. and Geiger, C.A. (1993) Andradite crystal chemistry, dynamic X-site disorder and structural strain in silicate garnets. *European Journal of Mineralogy*, **5**, 59–71.

Bastin, G.F., van Loo, F.J.J. and Heijlingers, H.J.M. (1984) Evaluation of the use of Gaussian φ(ρz) curves in quantitative electron probe microanalysis: a new optimization. *X-ray Spectrometry*, **13**, 91–97.

Bastin, G.F., Heijlingers, H.J.M. and van Loo, F.J.J. (1986) A further improvement in the Gaussian φ(ρz) approach for matrix correction in quantitative electron probe microanalysis. *Scanning*, **8**, 45–67.

Baur, H. (1974) The geometry of polyhedral distortions. Predictive relationships for the phosphate group. *Acta Crystallographica*, **B30**, 1195–1215.

Bermanec, V., Holtstam, D., Sturman, D., Criddle, A.J., Back, M.E. and Šavničar, S. (1996) Nežilovite, a new member of the magnetoplumbite group, and the crystal chemistry of magnetoplumbite and hibonite. *The Canadian Mineralogist*, **34**, 1287–1297.

Bischoff, A., Keil, K. and Stöffler, D. (1985) Perovskite-hibonite-spinel-bearing inclusions and aluminium-rich chondrules and fragments in enstatite chondrites. *Chemie der Erde*, **44**, 97–106.

Brese, N.E. and O'Keeffe, M. (1991) Bond-valence parameters for solids. *Acta Crystallographica*, **B47**, 192–197.

Brown, I.D. and Altermatt, D. (1985) Bond-valence parameters obtained from a systematic analysis of the inorganic crystal structure database. *Acta Crystallographica*, **B41**, 244–247.

Bruker (1999) *SMART and SAINT-Plus*. Versions 6.01. Bruker AXS Inc., Madison, Wisconsin, USA.

Büchel, G., Buhr, A., Gierisch, D. and Racher, R.P. (2005) Alkali- and CO-resistance of dense hexaluminate Bonite. *48th Internationales Feuerfest-Kolloquium*, 2005, Aachen, pp. 208–214.

Burns, R.G. and Burns, V.M. (1984) Crystal chemistry of meteoritic hibonites. Proceedings of the Fifteenth Lunar and Planetary Science Conference, Part 1. *Journal of Geophysical Research*, **89**, C313–C321.

Cao, Z., Qin, S., Bi, Y. and Wang, J. (1997) The discovery and preliminary study of hibonite from Handa-Xingtai Area, Hebei Province. *Acta Petrologica et Mineralogica*, **16**, 353–356 (Chinese with English abstract).

Collongues, R., Gourier, D., Kahn-Harari, A., Lejus, A.M., Théry, J. and Vivien, D. (1990) Magnetoplumbite-related oxides. *Annual Review of Materials Research*, **20**, 51–82.

Curien, H., Guillemin, C., Orcel, J. and Steinberg, M. (1956) La hibonite, norvelle espèce minérale. *Comptes Rendus Hebdomadaires des Seances de l'Academie des Sciences*, **242**, 2845–2847 (in French).

Fahey, A.J., Goswani, J.N., McKeegan, K.D. and

Zinner, E. (1987) ^{26}Al, ^{244}Pu, ^{50}Ti, REE and trace element abundances in hibonite grains from CM and CV meteorites. *Geochimica et Cosmochimica Acta*, **51**, 329–350.

Farrugia, L.J. (1999) *WinGX* suite for small-molecule single-crystal crystallography. *Journal of Applied Crystallography*, **32**, 837–838.

Graetsch, H. and Gebert, W. (1994) Positional and thermal disorder in the trigonal bipyramid of magnetoplumbite structure type $SrGa_{12}O_{19}$. *Zeitschrift für Kristallographie*, **209**, 338–342.

Hainschwang, T., Notari, F., Massi, L., Armbruster, T., Rondeau, B., Fritsch, E. and Nagashima, M. (2010) Hibonite: A new gem mineral. *Gems & Gemology*, **46**, 135–138.

Hazen, R.M. and Prewitt, C.T. (1977) Effects of temperature and pressure on interatomic distances in oxygen-based minerals. *American Mineralogist*, **62**, 309–315.

Holtstam, D. (1996) Iron in hibonite: a spectroscopic study. *Physics and Chemistry of Minerals*, **23**, 452–460.

Hummel, W., Hauser, J. and Bürgi, H.B. (1990) PEANUT: Computer graphics program to represent atomic displacement parameters. *Journal of Molecular Graphics*, **8**, 214–220.

Iyi, N., Takekawa, S. and Kimura, S. (1989) Crystal chemistry of hexaaluminates: β-alumina and magnetoplumbite structures. *Journal of Solid State Chemistry*, **83**, 8–19.

Kato, K. and Saalfeld, H. (1968) Verfeinerung der Kristallstruktur von $CaO{\cdot}6Al_2O_3$. *Neues Jahrbuch für Mineralogie*, *Abhandlungen*, **109**, 192–200.

Keil, K. and Fuchs, L.H. (1971) Hibonite-bearing microspherules: A new type of refractory inclusions with large isotopic anomalies. *Geochimica et Cosmochimica Acta*, **55**, 367–379.

Kimura, K., Ohgaki, M., Tanaka, K., Morikawa, H. and Marumo, F. (1990) Study of the bipyramidal site in magnetoplumbite-like compounds, $SrM_{12}O_{19}$ (M = Al, Fe, Ga). *Journal of Solid State Chemistry*, **87**, 186–194.

Kimura, M., El Goresy, A., Palme, H. and Zinner, E. (1993) Ca-Al-rich inclusions in the unique chondrite ALH 85085 – petrology, chemistry, and isotopic composition. *Geochimica et Cosmochimica Acta*, **57**, 2329–2359.

Kockegey-Lorenz, R., Buhr, A. and Racher, R.P. (2005) Industrial application experiences with microporous calcium hexaluminate insulating material SLA-92. *48th Internationales Feuerfest-Kolloquium, 2005*, Aachen, pp. 66–70.

Kohn, J.A. and Eckart, D.W. (1964) New hexagonal ferrite, establishing a second structural series. *Journal of Applied Physics*, **35**, 968–969.

Kreber, E., Gonser, U. and Trautwein, A. (1975) Mössbauer measurements of the bipyramidal lattice site in $BaFe_{12}O_{19}$. *The Journal of Physics and Chemistry of Solids*, **36**, 263–265.

Kunz, M. and Armbruster, T. (1990) Difference displacement parameters in alkali feldspars: Effects of (Si,Al) order-disorder. *American Mineralogist*, **75**, 141–149.

Kuzmin, A.M. (1960) Högbomite from Gornaya Shoriya. *Geologiya i Geofizika*, **4**, 63–75 (in Russian).

Liu, M.-C., McKeegan, K.D. and Davis, A.M. (2006) Magnesium isotopic compositions of CM hibonite grains. *Lunar and Planetary Science XXXVII* (Abstract, p. 2428).

Liu, M.-C., McKeegan, K.D., Davis, A.M. and Ireland, T.R. (2007) Magnesium-26 deficits in CM hibonite grains: Nucleosysthetic, galactic chemical evolution, or spallogenic? *Lunar and Planetary Science XXXVIII* (Abstract, p. 2253).

Liu, M.-C., Nittler, L.R., Alexander, C.M.O'D. and Lee, T. (2009) A search for internal ^{26}Al isochrones in CM hibonite. *40th Lunar and Planetary Science Conference* (Abstract, p. 1739).

Liu, M.-C. and McKeegan, K.D. (2009) On an irradiation origin for magnesium isotope anomalies in meteoritic hibonite. *The Astrophysical Journal*, **697**, L145–L148.

Ma, C. (2010) Hibonite-(Fe), $(Fe,Mg)Al_{12}O_{19}$, a new alteration mineral from the Allende meteorite. *American Mineralogist*, **95**, 188–191.

Maaskant, P., Coolen, J.J.M. and Burke, E.A.J. (1980) Hibonite and coexisting zoisite and clinozoisite in a calc-silicate granulite from southern Tanzania. *Mineralogical Magazine*, **43**, 995–1003.

Makide, K., Nagashima, K., Krot, A.N. and Huss, G.R. (2009) Oxygen isotopic compositions of solar, micrometer-sized corundum, hibonite and spinel grains in acid-resistant residues from ordinary and carbonaceous chondrites. *40th Lunar and Planetary Science Conference* (Abstract, p. 2079).

Momma, K. and Izumi, F. (2008) VESTA: a three-dimensional visualization system for electronic and structural analysis. *Journal of Applied Crystallography*, **41**, 653–658.

Nakamura, T.M., Sugiura, N., Kimura, M., Miyazaki, A. and Krot, A.N. (2007) Condensation and aggregation of solar corundum and corundum-hibonite grains. *Meteoritics and Planetary Science*, **42**, 1249–1265.

Obradors, X., Collomb, A., Pernet, M., Samaras, D. and Joubert, J.C. (1985) X-ray analysis of the structural and dynamic properties of $BaFe_{12}O_{19}$ hexagonal ferrite at room temperature. *Journal of Solid State Chemistry*, **56**, 171–181.

Packwood, R.H. and Brown, J.D. (1981) A Gaussian expression to describe $\phi(\rho z)$ curves for quantitative electron probe microanalysis. *X-ray Spectrometry*,

10, 138–146.

Rakotondrazafy, M.A.F., Moine, B. and Cuney, M. (1996) Mode of formation of hibonite ($CaAl_{12}O_{19}$) within the U-Th skarns from the granulites of S-E Madagascar. *Contributions to Mineralogy and Petrology*, **123**, 190–201.

Russell, S.S., Huss, G.R., Fahey, A.J., Greenwood, R.C., Hutchison, R. and Wasserburg, G.J. (1998) An isotopic and petrologic study of calcium-aluminum-rich inclusions from CO3 meteorites. *Geochimica et Cosmochimica Acta*, **62**, 689–714.

Sánchez-Herencia, A.J., Moreno, R. and Baudín, C. (2000) Fracture behaviour of alumina-calcium hexaluminate composites obtained by colloidal processing. *Journal of the European Ceramic Society*, **20**, 2575–2583.

Sandiford, M. and Santosh, M. (1991) A granulite facies kalsilite-leucite-hibonite association from Punalur, Southern India. *Mineralogy and Petrology*, **43**, 225–2360.

Santosh, M., Sandiford, M. and Reed, S.J.B. (1991) Zoned hibonites from Punalur, South India. *Mineralogical Magazine*, **55**, 159–162.

Shannon, R.D. (1976) Revised effective ionic radii and systematic studies of interatomic distances in halides and chalcogenides. *Acta Crystallographica*, **A32**, 751–767.

Sheldrick, G.M. (1996) *SADABS*. University of Göttingen, Germany.

Sheldrick, G.M. (2008) A short history of SHELX. *Acta Crystallographica*, **A64**, 112–122.

Simon, S.B., Grossman, L., Hutcheon, I.D., Phinney, D.L., Weber, P.K. and Fallon, S.J. (2006) Formation of spinel-, hibonite-rich inclusions found in CM2 carbonaceous chondrites. *American Mineralogist*, **91**, 1675–1687.

Stroud, R.M., Nittler, L.R. and Alexander, C.M.O'D. (2008) Transmission electron microscopy of a presolar supernova hibonite grain. *Lunar and Planetary Science XXXIX* (Abstract, p. 1778).

Trueblood, K.N. (1978) Analysis of molecular motion with allowance for intramolecular torsion. *Acta Crystallographica*, A34, 950–954.

Ulianov, A. and Kalt, A. (2006) Mg-Al sapphirine- and Ca-Al hibonite-bearing granulite xenoliths from the Chyulu Hills volcanic field, Kenya. *Journal of Petrology*, **47**, 901–927.

Ulianov, A., Kalt, A. and Pettke, T. (2005) Hibonite, $Ca(Al,Cr,Ti,Si,Mg,Fe^{2+})_{12}O_{19}$, in granulite xenoliths from the Chyulu Hills volcanic field, Kenya. *European Journal of Mineralogy*, **17**, 357–366.

Utsunomiya, A., Tanaka, K., Morikawa, H., Marumo, F. and Kojima, H. (1988) Structure refinement of $CaO{\cdot}6Al_2O_3$. *Journal of Solid State Chemistry*, **75**, 197–200.

Yakovlevskaya, T.A. (1961) Hibonite from Gornaya Shoria. *Zapiski Vsesoyuzngo Mineralogischekogo Obshchestava*, **90**, 458–461 (in Russian).